# Mechanistic Insights into Hydroformylation Catalyzed by Cationic Cobalt(II) Complexes: In Silico Modification of the Catalyst System

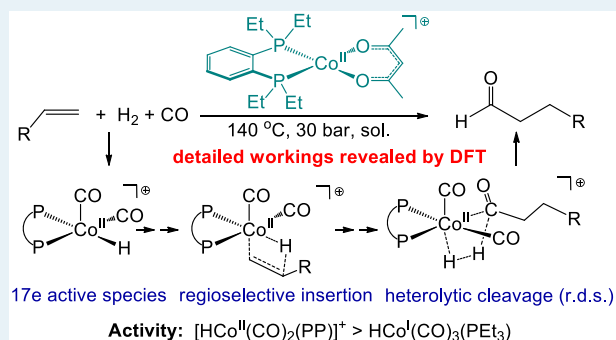Jiandong Guo, Dongju Zhang, and Xiaotai Wang*

ACCESS | Metrics & More | Article Recommendations | SI Supporting Information

**ABSTRACT:** The hydroformylation reaction is used on a large industrial scale to convert olefins and synthesis gas ($CO + H_2$) into aldehydes. Researchers have recently discovered that a class of cationic Co(II) complexes of the formula $[Co^{II}(PP)(acac)]^+$ (PP = diphosphine, acac = acetylacetonate) can catalyze hydroformylation with activity approaching that of the widely used rhodium catalysts (Hood, D. M. et al. *Science* 2020, 367, 542−548). This density functional theory (DFT) study reveals the detailed workings of the cationic Co(II) catalyst system. The precatalyst $[Co^{II}(PP)(acac)]^+$ is initiated by reacting with $H_2$ and CO to generate active species $[HCo^{II}(CO)_2(PP)]^+$. In comparison with the 18-electron neutral Co(I) catalytic species $HCo^I(CO)_3(PR_3)$, these cationic Co(II) species, with their unique 17-electron and square pyramidal structure,



**detailed workings revealed by DFT**

17e active species   regioselective insertion   heterolytic cleavage (r.d.s.)

**Activity:** $[HCo^{II}(CO)_2(PP)]^+ > HCo^I(CO)_3(PEt_3)$

invoke a lower-energy pathway through different elementary steps such as associative alkene uptake and heterolytic $H_2$ cleavage. The regioselectivity for linear aldehyde products is due to a combination of electronic and steric effects that favor the anti-Markovnikov insertion of a terminal alkene into the Co−H bond. DFT calculations predict that addition of $PMe_3$ would facilitate the precatalyst initiation, thereby decreasing the reaction temperature or shortening the induction period. The insights gained by this theoretical study can be useful for the further development of hydroformylation catalysts.

**KEYWORDS:** *cobalt catalysis, hydroformylation, cationic Co(II) catalyst system, DFT studies, reaction mechanism*
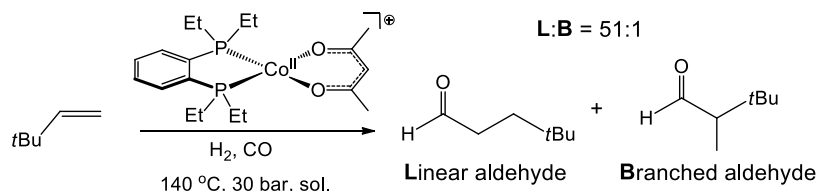
## 1. INTRODUCTION

Hydroformylation, also known as the oxo process, is a transition metal-catalyzed homogeneous reaction that converts alkenes, carbon monoxide (CO), and hydrogen ($H_2$) into aldehydes.[1] Today it is one of the most widely used homogeneous industrial processes in the world, turning out more than 10 million metric tons of products per year.[2] The original hydroformylation catalyst, discovered in 1938, was a cobalt(I) complex, $HCo(CO)_4$.[3] High partial pressure of CO must be maintained for $HCo(CO)_4$ to function optimally, or it would decompose to cobalt metal as the temperature increases. This catalyst was later modified with phosphines to form the more stable $HCo(CO)_3(PR_3)$ system, which could work at lower pressures.[4] However, the phosphine ligand reduces catalyst activity, so the reaction requires higher temperatures and higher catalyst concentrations. Since the 1970s, rhodium-based catalysts have been developed for hydroformylation, which are more active and operate under lower pressures and temperatures.[5] However, rhodium is one of the most expensive precious metals, and the continuous need for precious-metal catalysts raises economic concerns and has environmental implications. A contemporary approach for the development of more sustainable catalysis is to use Earth-abundant 3d transition metals.[6]

The Stanley group has recently reported a remarkable discovery that a class of cationic cobalt(II) complexes can catalyze hydroformylation with activity approaching that of the rhodium catalysts.[7] These square planar cationic Co(II) $d^7$ chelates are formulated as $[Co(PP)(acac)]^+$ (PP = diphosphine, acac = acetylacetonate), and a sample catalytic reaction is shown in Scheme 1.[7] Stanley et al. proposed a mechanistic outline for the hydroformylation effected by the cationic Co(II) catalyst system (Scheme 2).[7] The Co(II) complex cation **A**, the precatalyst, is initially activated by reacting with the CO and $H_2$ substrates to give the 15-electron Co(II) carbonyl hydride complex **B**. Coordination by CO transforms **B** into the 17-electron complex **C**, which can interconvert with the isomer **E** through the less stable 19-electron complex **D**. Complex **E** is envisioned to coordinate an alkene to start a catalytic cycle similar to that proposed for the $HCo(CO)_4$-catalyzed hydroformylation.[8] Yet there is an important

**Scheme 1. Co(II)-Catalyzed Hydroformylation**



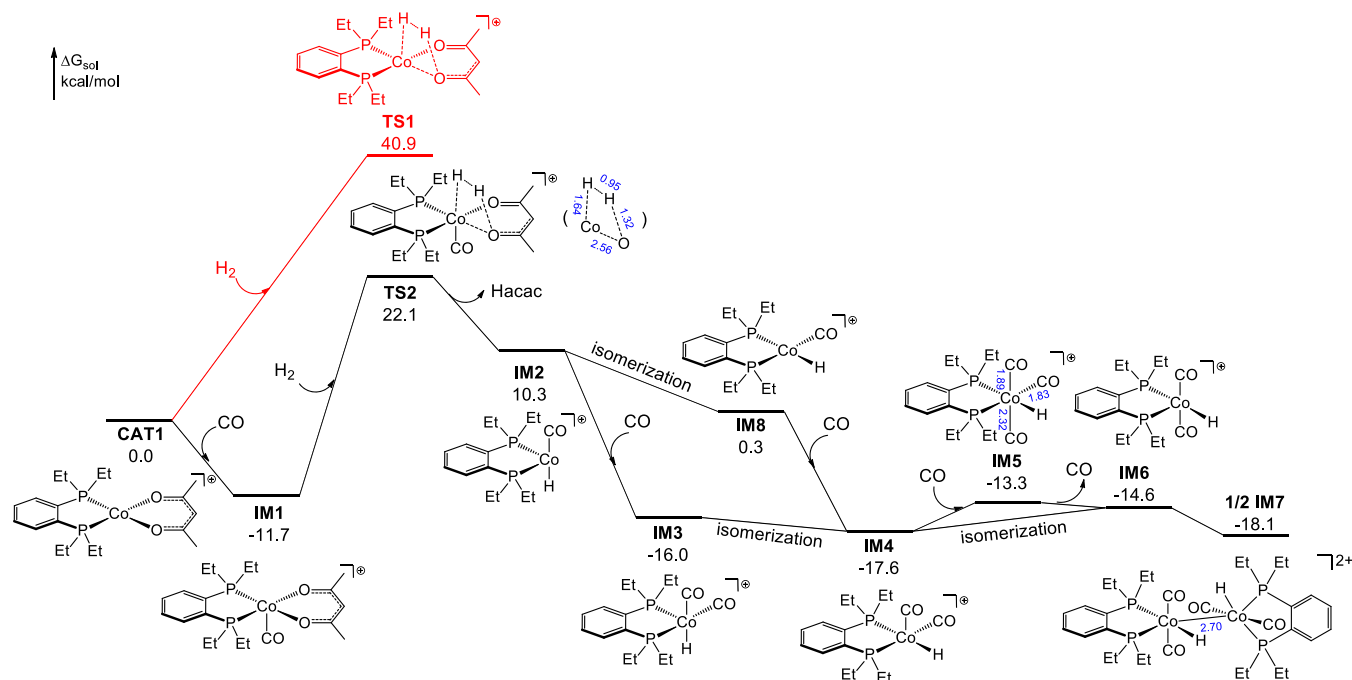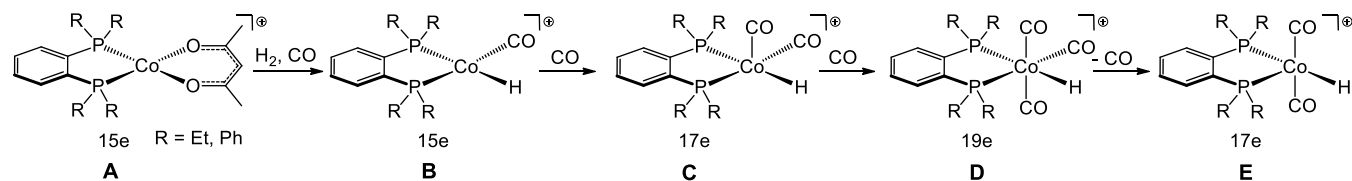**Scheme 2. Co(II) Species in Hydroformylation**





**Figure 1.** Free energy profile for the initiation process of the precatalyst. Selected bond distances in blue font are given in Å (the same below).

difference: H$_2$ would likely react with the Co(II) acyl intermediate by heterolytic cleavage to eliminate the aldehyde product and regenerate the cationic Co(II) catalyst, as an oxidative addition of H$_2$ to Co(II) to form a Co(IV) dihydride complex would be unlikely. In addition, Stanley et al. performed some density functional theory (DFT) calculations to (1) locate **A**, **B**, **C**, and **D** as energy minima and (2) evaluate the free energy changes for the **A** → **B**, **B** → **C**, and **C** → **D** processes.

The discovery of the cationic Co(II) catalyst system represents a major advance for the field of hydroformylation chemistry, which has inspired our interest. There are a significant number of computational studies on Co(I)-catalyzed alkene hydroformylation.[9−14] We wish to study the new cationic Co(II) catalyst system by means of extensive DFT computations. We seek to elucidate the detailed mechanism of the reaction shown in Scheme 1[15] and gain deep insights into the greater activity of this cationic Co(II) catalyst system in comparison with the neutral Co(I) system. The insights can be helpful for the further development of

cobalt-based hydroformylation catalysts. Specific questions addressed by this study include the initial activation of the precatalyst [Co(PP)(acac)]$^+$, the various reaction pathways through the 17-electron complexes like **E** and **C**, the dimerization of the 17-electron species, the origins of the regioselectivity favoring linear aldehydes, the factors that set apart the Co(II) and Co(I) catalyst systems, and the theoretical modification of the Co(II) catalyst system.

## 2. COMPUTATIONAL METHODS

DFT calculations were performed with Gaussian 09.[16] All calculations were with the ultrafine integration grid and the keyword acc2e = 11. Full molecular systems were used without any truncations or symmetry constraints. Geometries were optimized and characterized by frequency calculations to be energy minima (zero imaginary frequencies) or transition states (only one imaginary frequency) at the M06-L[17]/BS1 level in the gas phase, with BS1 designating a mixed basis set of SDD[18] for cobalt and 6-31G(d,p) for other atoms. The
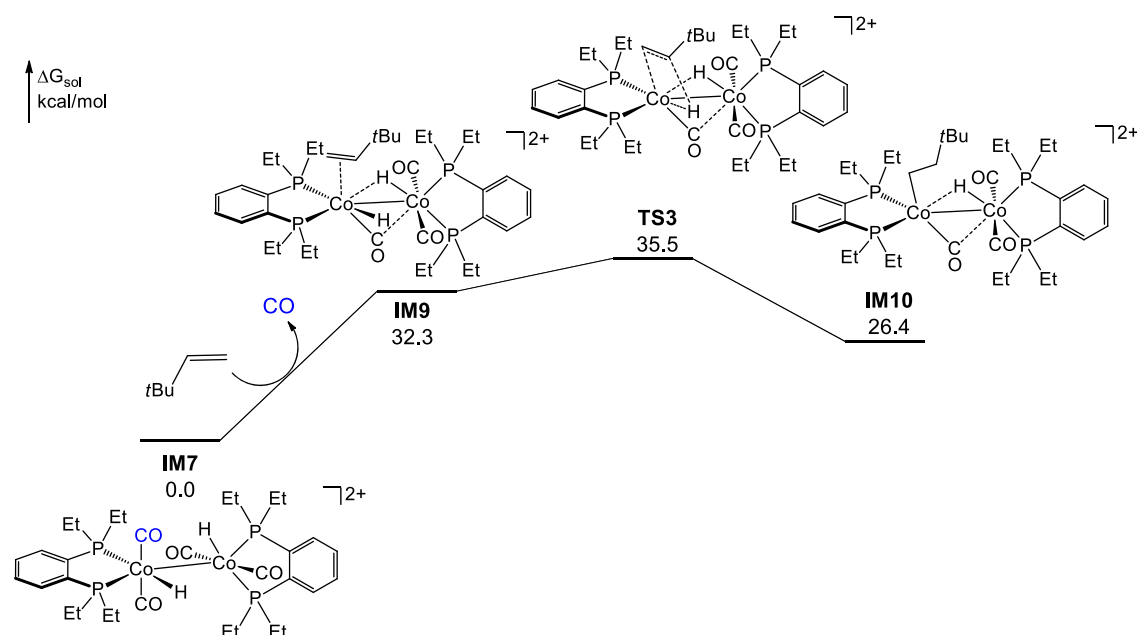
**Figure 2.** Free energy profile for the alkene insertion into the dimer **IM7**.

energies were then refined by M06-L/BS2//M06-L/BS1 single-point energy calculations in solution using the SMD solvation model,[19,20] with BS2 denoting a mixed basis set of SDD for cobalt and 6-311++G(d,p) for other atoms. The refined energies were converted to zero-point energy-corrected free energies at 298.15 K and 1 atm, using the M06-L/BS1 harmonic frequencies. Entropy corrections were then made to the free energies on the basis of "the theory of free volume"; that is, for 2-to-1 (or 1-to-2) reactions, a correction of −2.6 (or 2.6) kcal/mol was applied.[21] Natural population analyses (NPA) were performed on selected structures via M06-L/BS2//M06-L/BS1 computations in solution using the SMD model.

The doublet spin state was experimentally determined for a $[Co(PP)(acac)]^{+}$ complex via electron paramagnetic resonance (EPR),[7] which was supported by our calculations on **CAT1**.[22] The other Co(II) d[7] species, all of them derived from **CAT1** and supported by strong-field ligands such as CO and phosphines, were computed as low-spin doublets.[23] Benchmark calculations were performed on the key transition states with M06-L-D3[24] and M06,[25] as well as with solvation effects included in M06-L geometry optimizations and frequency calculations; the results obtained with different methods showed good consistency (Figure S2).

## 3. RESULTS AND DISCUSSION

**3.1. Precatalyst Initiation.** As shown in Figure 1, the direct σ-bond metathesis between the cationic Co(II) precatalyst **CAT1** and $H_2$ would face an exceedingly high energy barrier (**TS1**) at 40.9 kcal/mol, so this pathway is not considered further. The square planar chelate geometry of **CAT1** appears to prevent the cis-constrained oxidative addition of $H_2$, as no such transition state or product could be found. Coordination by CO turns **CAT1** into the more stable 17-electron complex **IM1**, which opens up a lower-energy pathway for heterolytic cleavage of $H_2$ via the four-membered transition state **TS2**. **TS2** is 33.8 kcal/mol with respect to **IM1**, an energy barrier that can be overcome at the reaction temperature (140 °C). With the extrusion of

acetylacetone, **TS2** proceeds to the seesaw-shaped 15-electron Co(II) carbonyl hydride complex **IM2**. Coordination by CO converts **IM2** into the 17-electron square pyramidal complex **IM3**, with a large thermodynamic driving force ($\Delta G = -26.3$ kcal/mol).

**IM3** can isomerize to **IM4** (an equivalent to the **C** complex above). Further coordination by CO to **IM4** is endergonic by 4.3 kcal/mol, and the resulting, less stable 19-electron complex **IM5** (an equivalent to the **D** complex above) can lose a CO ligand to yield **IM6** (an equivalent to the **E** complex above). Note that **IM4** can also isomerize to **IM6**. The dimerization of **IM6** is exergonic ($\Delta G = -3.5$ kcal/mol), affording the closed-shell dinuclear complex **IM7** with a Co−Co bond at 2.70 Å.[26] We have also located the square planar complex **IM8** (an equivalent to the **B** complex above) which can be viewed as resulting from the isomerization of **IM2**. The computed energetics show that the dimer **IM7** is the most stable species generated in the initiation process and that **IM3**, **IM4**, **IM6**, and **IM7** equilibrate in the system. Thus, **IM7** is taken as the catalyst resting state and its relative free energy is set to zero in the subsequent calculations. **IM3**, **IM4**, and **IM6** are the 17-electron complexes with a vacant coordination site cis to the Co−H bond that can be occupied by an alkene to start a hydroformylation process.

**3.2. Catalytic Pathways.** Let us first consider the dimer **IM7** for the catalytic cycle (Figure 2). Substitution of t-butylethylene for one CO ligand converts **IM7** into **IM9**, and this process is thermodynamically uphill ($\Delta G = 32.3$ kcal/mol). The large endergonicity is attributed to t-butylethylene being a poorer ligand than CO for Co(II) as well as to the steric strain in **IM9**. Analysis of the optimized geometry of **IM9** reveals four significant steric repulsions occurring between nonbonded H atoms at a distance less than 2.40 Å (two times the van der Waals radius of hydrogen 1.20 Å), which add up to a severe destabilizing effect on **IM9** (Figure S3). The steric congestion becomes worse in **TS3**, the transition state of t-butylethylene migratory insertion into the Co−H bond (Figure S3), which is 35.5 kcal/mol with respect to **IM7**. Owing to this
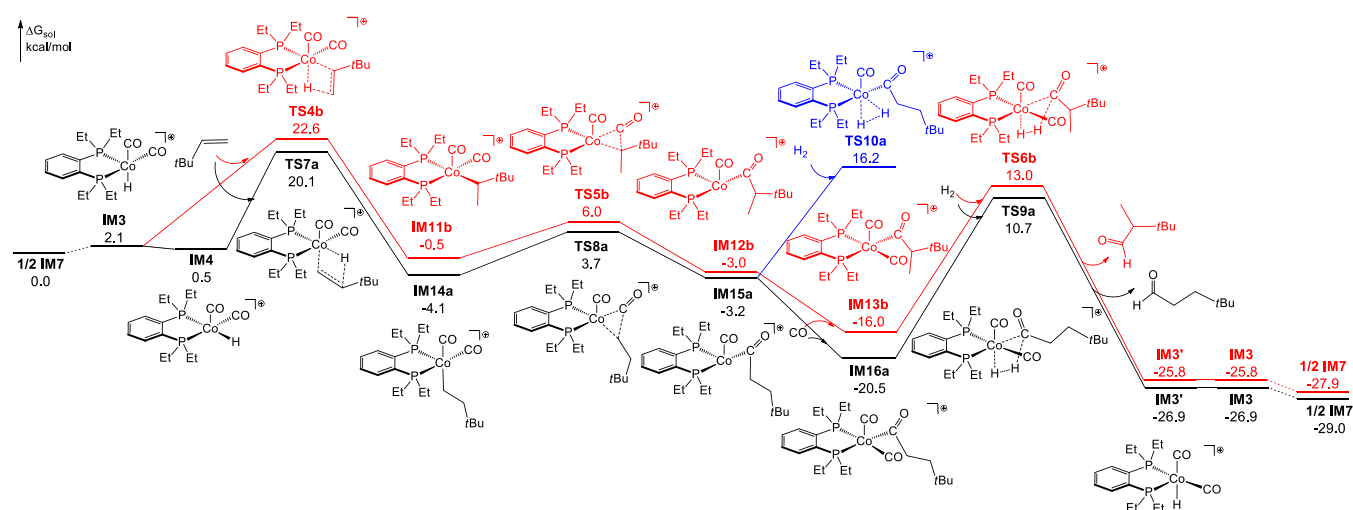
**Figure 3.** Free energy profile for the hydroformylation pathways leading to the linear (black) and branched (red) aldehydes. The mirror inverts **IM3'** and **IM3** can easily interconvert.
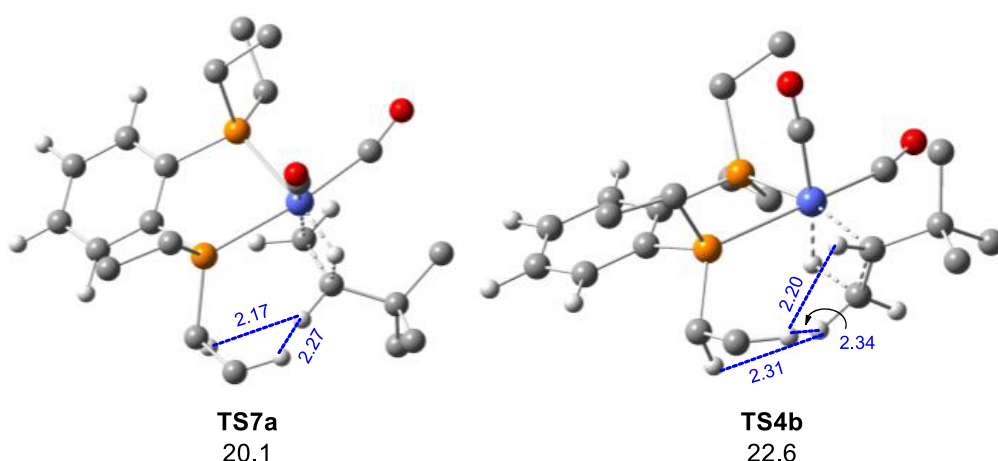


**Figure 4.** Optimized geometries of **TS7a** and **TS4b** showing steric repulsions between nonbonded H atoms. Certain irrelevant H atoms are omitted for clarity.

high energy barrier, the dimeric pathway is disfavored and not considered further.

Considering that each of the monomers **IM3**, **IM4**, and **IM6** can take up *t*-butylethylene, we have computed various possible hydroformylation pathways through these species (Figures S4−S6). The most favorable pathways leading to the linear and branched aldehydes are through *t*-butylethylene insertion into **IM4** and **IM3**, respectively, as shown in Figure 3. The regioselectivity stems from the different orientations of the unsymmetrical *t*BuCH=CH$_2$ toward the Co−H bond in the transition states **TS7a** and **TS4b**,[27] which proceed in the anti-Markovnikov (black) and Markovnikov (red) pathways, respectively. In comparison with **TS3**, **TS7a** and **TS4b** are much lower energy barriers. They proceed respectively to **IM14a** and **IM11b**, the alkyl-Co(II) carbonyl complexes, which then undergo facile intramolecular CO migratory insertion via **TS8a** and **TS5b** to form the 15-electron acyl-Co(II) carbonyl complexes **IM15a** and **IM12b**, respectively. Coordination by CO converts **IM15a** and **IM12b** into the more stable 17-electron **IM16a** and **IM13b**. These complexes metathesize with H$_2$ via **TS9a** and **TS6b** to deliver the linear and branched aldehydes, respectively. The resulting 17-electron Co(II) intermediate **IM3'** (the mirror invert of

**IM3**) converts to the catalyst resting state **IM7** through isomerization and dimerization to formally close the catalytic cycle. The overall reaction is thermodynamically favorable with a large driving force (29 kcal/mol). The alkene insertions via **TS7a** and **TS4b** are the regioselectivity-determining steps, and the energy gap between **TS7a** and **TS4b** (2.5 kcal/mol) explains that the linear aldehyde resulting from **TS7a** is the major product. The heterolytic cleavage of H$_2$ by **IM16a** via **TS9a** is the rate-determining step of the favored, anti-Markovnikov pathway, along which the largest energy span[28] is 31.2 kcal/mol (**TS9a−IM16a**). On another note, we have traced **TS10a**, the transition state for the oxidative addition of H$_2$ to **IM15a**. **TS10a** is higher in energy than **TS9a** by 5.5 kcal/mol, and this result lends support to the experimentalists' thought that the oxidative addition of H$_2$ to a Co(II) acyl species to form a Co(IV) dihydride complex would be unlikely.

In the following sections, we will discuss the structural origins of the regioselectivity, compare with Co(I)-promoted hydroformylation to gain more insight into the cationic Co(II) catalyst, and attempt to modify the Co(II) catalyst system computationally.

**3.3. Origins of Regioselectivity.** As shown in Figure 3, the regioselectivity is manifested by the energy gap of 2.5 kcal/

mol between **TS7a** and **TS4b**, the transition states that induce the irreversible alkene insertions and determine the linear/branched product selectivity.

A recent computational study on Co(I)-catalyzed hydroformylation of terminal alkenes ascribed the linear product selectivity mainly to steric effects.[29] Accordingly, we have first examined the optimized structures of **TS7a** and **TS4b** to identify steric bias. Indeed, there is in **TS4b** more steric hindrance as shown by van der Waals repulsions between nonbonded H atoms at a distance less than 2.40 Å (Figure 4). However, the steric bias does not seem large enough to explain fully the energy gap between **TS7a** and **TS4b**, which have led us to investigate the electronic effects.

In an early theoretical study on the $HCo(CO)_4$-catalyzed hydroformylation of propene, Grima et al. proposed that the regioselectivity originates from the electrostatic dipole−dipole interaction between Co−H and C=C that favors the anti-Markovnikov insertion.[10] We have analyzed the natural charges on the atoms of the Co−H and C=C bonds in **IM4/IM3** and $tBuCH=CH_2$ (Figure 5). The Co−H bond in **IM4/IM3** has a



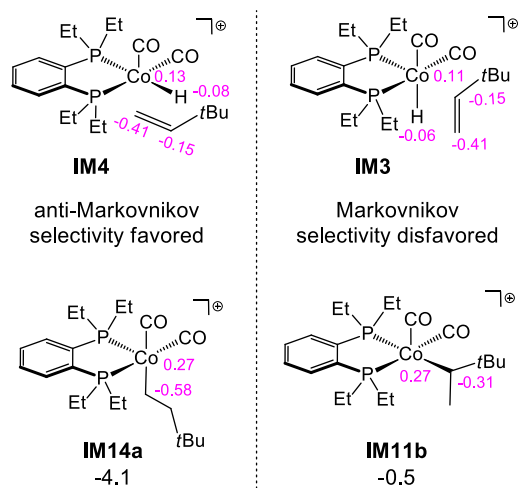**Figure 5.** Orientations of *t*-butylethylene toward the Co−H bond of **IM4/IM3** and geometries and energies of corresponding alkene insertion intermediates. The numbers shown in purple font denote natural charges on selected atoms.

partial positive charge on Co (0.13/0.11) and a negative charge on H (−0.08/−0.06). The C=C bond in $tBuCH=CH_2$ has partial negative charges on both C atoms, but the charge on the terminal carbon (−0.41) is significantly more negative than that on the internal carbon (−0.15) due to the *t*-butyl group's electron-donating effect. These natural charge distributions suggest that the $Co^{\delta+}-C^{\delta-}$ (terminal) attractive interaction between **IM4** and $tBuCH=CH_2$ in the anti-Markovnikov orientation is stronger than the $Co^{\delta+}-C^{\delta-}$ (internal) attractive interaction between **IM3** and $tBuCH=CH_2$ in the Markovnikov orientation. Furthermore, the repulsive interaction between $C^{\delta-}$ (internal) and Co-bound $H^{\delta-}$ in the anti-Markovnikov orientation is smaller than that between $C^{\delta-}$ (terminal) and Co-bound $H^{\delta-}$ in the Markovnikov orientation. In addition, the anti-Markovnikov alkene insertion intermediate **IM14a** has a stronger cobalt/alkyl charge attraction than the Markovnikov intermediate **IM11b** does, which contributes to the higher stability of **IM14a** versus **IM11b** (Figure 5). Therefore, the electronic factors favor the anti-Markovnikov insertion of *t*-butylethylene into **IM4** over

the Markovnikov insertion of *t*-butylethylene into **IM3**. This finding is consistent with the charge effect on the regioselectivity of alkene insertion proposed by Grima et al.[10]

In summary, the cationic Co(II) catalyst, akin to other hydroformylation catalysts, is very selective to the linear aldehyde product for the substrate *t*-butylethylene, and the high regioselectivity arises from a combination of electronic and steric effects.[30]

### 3.4. Comparing the Co(II) and Co(I) Catalytic Activity.

Comparing the neutral Co(I) and cationic Co(II) catalysts in terms of computed hydroformylation profiles could shed light on the higher activity of the Co(II) system. Of the Co(I) systems $HCo(CO)_4$ and $HCo(CO)_3(PR_3)$, the latter would provide more appropriate benchmarking, as the Co(II) catalyst in question has a metal-bound diethylphosphino $(PEt_2)$ moiety. Thus, we choose to compute the most favorable $HCo(CO)_3(PEt_3)$-catalyzed pathway, then compare it with the pathway through the Co(II) species **IM4** as shown in Figure 3.

There are a total of eight conceivable trigonal bipyramidal and square pyramidal geometries of $HCo(CO)_3(PEt_3)$, but they converge to only two configurations after optimization: **Co$^I$1** and **Co$^I$2** (Figure 6). We have considered various
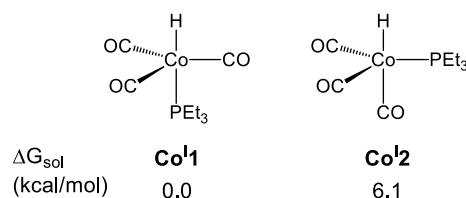


**Figure 6.** Computed structures and relative energies of two isomers of $HCo(CO)_3(PEt_3)$.

possible pathways of hydroformylation through **Co$^I$1** and **Co$^I$2**. The most favorable pathway, which leads to the linear aldehyde product as expected, is shown in Figure 7.

The 18-electron complex **Co$^I$1** would have to lose a CO ligand while binding the alkene, for which we have found two routes. The interchange route through **TS14** is disfavored because of the high energy barrier (39.3 kcal/mol). For the dissociative route through **IM20**, no transition state could be found between **Co$^I$1** and **IM20**. A potential energy surface scan along the Co−CO bond of **Co$^I$1** shows a monotonic increase in energy, suggesting that there is no transition state (Figure S7). The subsequent alkene coordination to **IM20** proceeds via **TS15** to form **IM21**, and **TS15** is lower than **TS14** by 2.3 kcal/mol. Alkene insertion into the Co−H bond via **TS16** affords the 16-electron Co(I) alkyl intermediate **IM22**, which then binds CO to form the more stable 18-electron complex **IM23**. Intramolecular CO insertion into the Co−C bond via **TS17** converts **IM23** to the 16-electron Co(I) acyl complex **IM24** with a weak Co···H(methylene) agostic interaction. Rotation about the Co−C(O) bond gives the conformer **IM25** with an open fifth coordination site for an incoming CO to occupy, and the resulting 18-electron **IM26** is much more stable. **IM26** must revert to **IM25** for $H_2$ to add oxidatively via **TS18** to give the Co(III) acyl hydride complex **IM27**. Reductive elimination from **IM27** via **TS19** provides the linear aldehyde product. **TS18** and **TS19** are, respectively, 33.1 and 36.7 kcal/mol relative to **IM26**. Yet the largest energy span along the computed profile is from **Co$^I$1** to **TS15**, 37.0 kcal/mol, suggesting that alkene addition to the coordinatively unsaturated **IM20** is the rate-determining step of this
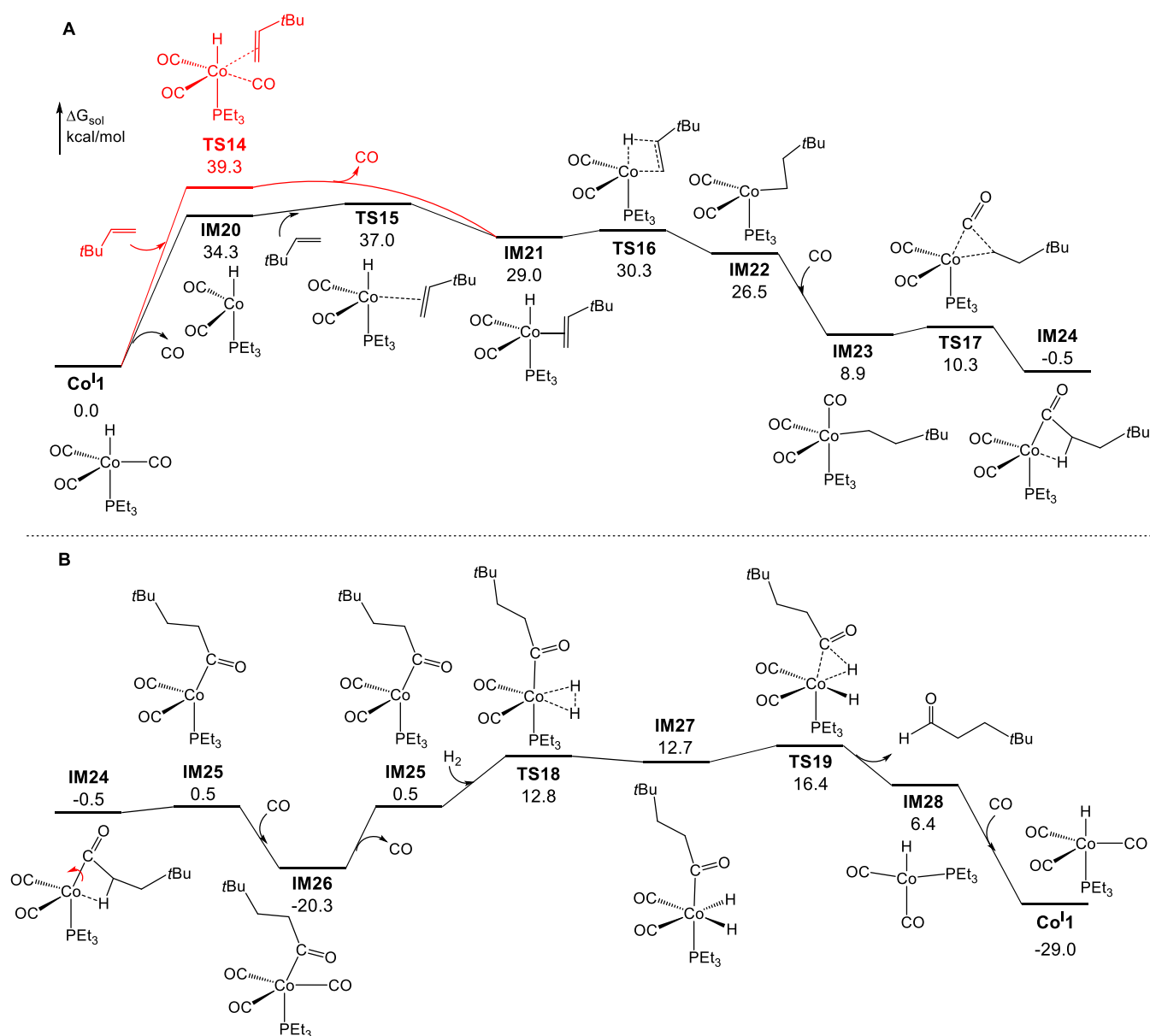
**Figure 7.** Free energy profile for the most favorable pathway of HCo(CO)$_3$(PEt$_3$)-catalyzed hydroformylation of *t*-butylethylene.

hydroformylation reaction. This outcome agrees with the thought that the dissociative substitution of alkene for CO in HCo(CO)$_3$(PBu$_3$) is rate-limiting in the hydroformylation mechanism.[31] It also agrees with the conclusion of a recent computational study on HCo(CO)$_4$-catalyzed hydroformylation of propene.[14b]

In the Co(II)-catalyzed pathway, the 17-electron Co(II) species **IM4** can take up *t*BuCH=CH$_2$ directly via **TS7a**, without the need to dissociate a CO ligand (Figure 3). The rate-determining step becomes the heterolytic cleavage of H$_2$ by the acyl-Co(II) complex **IM16a** via **TS9a**, which defines the largest energy span of 31.2 kcal/mol. This value is smaller than 37.0 kcal/mol, the largest energy span in the Co(I)-catalyzed pathway (Figure 7). The difference of 5.8 kcal/mol in apparent activation energy would entail a large ratio of reaction rates. In other words, the Co(II)-catalyzed hydroformylation would proceed much faster than the Co(I)-catalyzed reaction. This clearly accounts for the higher activity of the cationic Co(II)

species in comparison with the neutral Co(I) system HCo(CO)$_3$(PR$_3$).

**3.5. Theoretical Modification of the Co(II) Catalyst System.** As shown in Figure 1, the DFT calculations reveal a somewhat high energy barrier of 33.8 kcal/mol (**TS2−IM1**) for the activation of the precatalyst **CAT1**. Note that **IM1** and **TS2** are both cationic Co(II) complexes. Replacement of the axial CO ligand with a stronger σ donor could stabilize the transition state more than the precursor, thereby lowering the activation energy. Along these lines of thought, we have found the monodentate phosphine PMe$_3$ as a suitable additive to the system, which would expedite the initiation of **CAT1**, as shown in Figure 8. While **IM29** is lower than **IM1** by 0.7 kcal/mol, **TS20** is lower than **TS2** by 3.4 kcal/mol. Thus, the activation energy decreases from 33.8 to 31.1 kcal/mol. This change can result in lower temperatures and/or shorter induction periods for the catalytic reaction. We offer a reasonable insight into the relatively lower energy of **TS20**. In this transition state of heterolytic cleavage of H$_2$, the H$_2$ molecule is polarized,
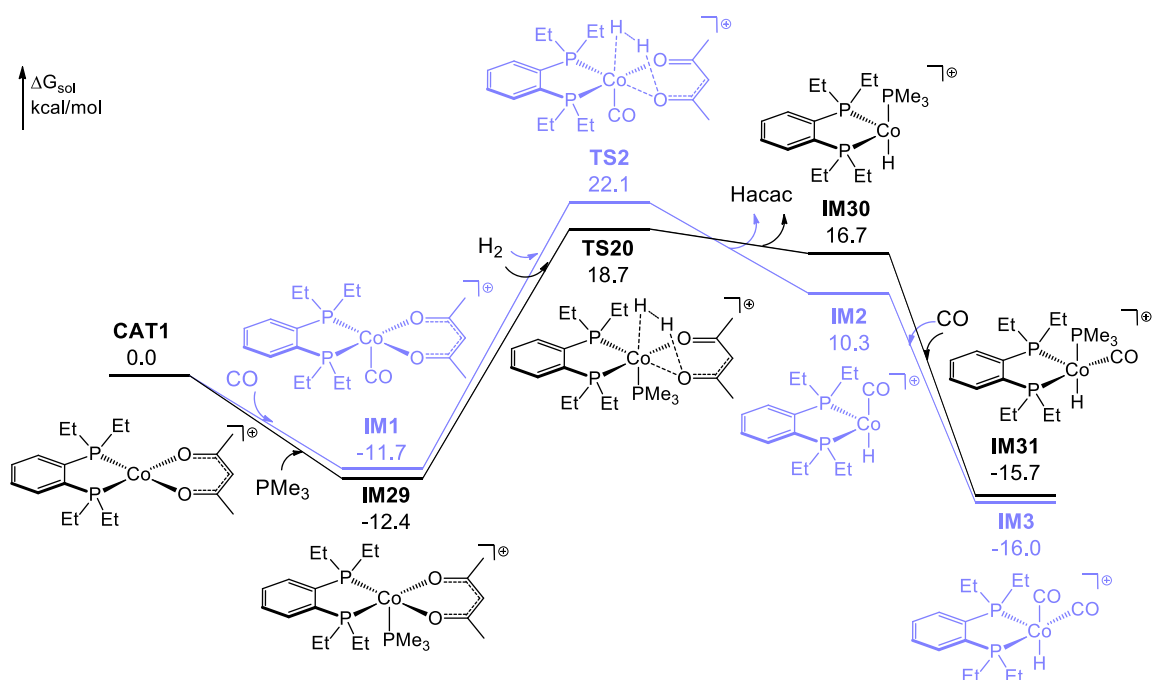
**Figure 8.** Energy profile comparing the CO- and PMe$_3$-assisted precatalyst initiations.



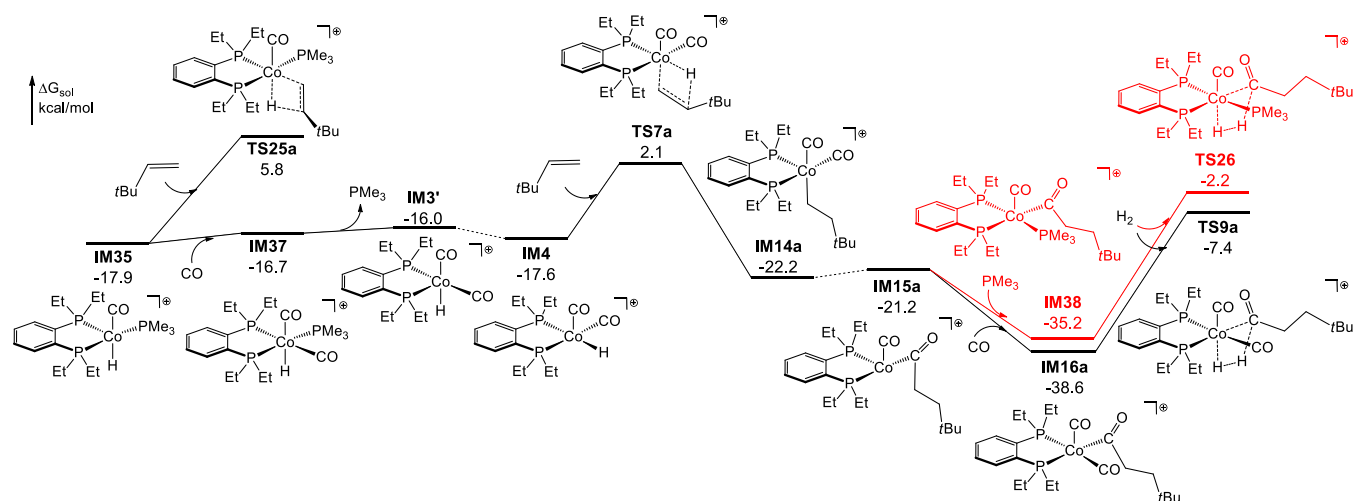**Figure 9.** Free energy profile for the **IM35**-catalyzed hydroformylation (see Figure 3 for the full pathway through **IM4**).

donating its protonic end to the acac ligand (a base) and its hydridic end to the Co(II) center. The proton donation to acac is particularly facilitated because coordination of the $\sigma$ donor PMe$_3$ to Co increases the electron density on acac. **TS20** proceeds to **IM30** which then converts to the more stable 17-electron **IM31** by CO coordination.

**IM31** can have five geometric isomers, namely, **IM32**–**IM36** (Figure S8). Complexes **IM31**–**IM35** all have a vacant coordination site cis to the Co–H bond, thus being potential active catalysts for hydroformylation. We have considered the insertion of *t*BuCH=CH$_2$ into each of **IM31**–**IM35** (Figure S9). **IM35** would introduce the lowest-energy transition state **TS25a** for the alkene insertion, but **TS25a** is still 3.7 kcal/mol higher than **TS7a** that bears no PMe$_3$ (Figure 9). There exists in **TS25a** steric hindrance induced by the presence of PMe$_3$ (Figure S10). These results suggest that, after the precatalyst initiation, the reaction would prefer to proceed with CO replacing PMe$_3$ to reach **IM4**, the precursor to **TS7a** (Figure

9), and the remainder of the pathway would be identical to that of the **IM4**-introduced hydroformylation pathway (Figure 3). Note that we considered and ruled out the PMe$_3$ rebound pathway through **IM38** and **TS26**. Thus, adding PMe$_3$ would not change the largest energy span (or apparent activation energy) in the hydroformylation phase.

In summary, our calculations suggest that addition of PMe$_3$ would facilitate the activation of the precatalyst [Co$^{II}$(PP)-(acac)]$^+$, thereby decreasing the reaction temperature or shortening the induction period. We intend this computationally informed idea to stimulate experimental investigation.[32]

**3.6. Conclusions.** We have utilized DFT computations to elucidate the mechanism of the newly developed hydroformylation reaction catalyzed by a class of cationic Co(II) complexes [Co(PP)(acac)]$^+$. **CAT1**, one such complex, promotes the regioselective hydroformylation of *t*-butylethylene. **CAT1** initially reacts with H$_2$ and CO to generate five-coordinate, 17-electron active complexes [HCo-

$(CO)_2(PP)]^+$. Two of these species, **IM4** and **IM3**, respectively introduce the most favorable hydroformylation pathways leading to the linear aldehyde (major product) and branched aldehyde (minor product). The regioselectivity is due to a combination of electronic and steric effects that favor the anti-Markovnikov insertion of $tBuCH=CH_2$ into the Co—H bond in **IM4**. The Co(II) acyl intermediate, which is derived from intramolecular CO insertion, activates $H_2$ by heterolytic cleavage to deliver the aldehyde product and regenerate the catalyst. This is the rate-determining step defining the largest energy span ($\delta G_1$) of the catalytic cycle

In contrast, the 18-electron neutral Co(I) catalyst HCo-$(CO)_3(PEt_3)$ must lose a CO ligand to bind the alkene substrate and the energy cost is so high that the ensuing alkene coordination becomes the rate-determining step defining the largest energy span ($\delta G_2$). The calculations reveal that $\delta G_1$ is considerably smaller than $\delta G_2$, thereby unraveling the higher catalytic activity of the cationic Co(II) system. In essence, the cationic Co(II) active species, with their unique 17-electron, five-coordinate, and square pyramidal structure, are capable of invoking a lower-energy pathway through different elementary steps such as associative alkene uptake and heterolytic $H_2$ cleavage. The calculations also suggest that adding $PMe_3$ to $[Co(PP)(acac)]^+$ would accelerate the activation of the precatalyst.

This DFT study provides deep insights into the workings of the new class of hydroformylation catalysts derived from cationic Co(II) diphosphine complexes. The computationally informed ideas can have implications for the further development of cobalt-based hydroformylation catalysts.

## ASSOCIATED CONTENT

### Ⓢ Supporting Information

The Supporting Information is available free of charge at https://pubs.acs.org/doi/10.1021/acscatal.0c03161.

Additional computational results and energies and Cartesian coordinates of the optimized structures (PDF)

## AUTHOR INFORMATION

### Corresponding Author

**Xiaotai Wang** — *Hoffmann Institute of Advanced Materials, Postdoctoral Innovation Practice Base, Shenzhen Polytechnic, Shenzhen 518055, P. R. China; Department of Chemistry, University of Colorado Denver, Denver, Colorado 80217-3364, United States;* ⓞ orcid.org/0000-0003-3310-3308; Email: xiaotai.wang@ucdenver.edu

### Authors

**Jiandong Guo** — *Hoffmann Institute of Advanced Materials, Postdoctoral Innovation Practice Base, Shenzhen Polytechnic, Shenzhen 518055, P. R. China; Institute of Theoretical Chemistry, School of Chemistry and Chemical Engineering, Shandong University, Jinan 250100, P. R. China*

**Dongju Zhang** — *Institute of Theoretical Chemistry, School of Chemistry and Chemical Engineering, Shandong University, Jinan 250100, P. R. China;* ⓞ orcid.org/0000-0002-6117-4958

Complete contact information is available at:
https://pubs.acs.org/10.1021/acscatal.0c03161

### Notes

## REFERENCES

(1) (a) Pospech, J.; Fleischer, I.; Franke, R.; Buchholz, S.; Beller, M. Alternative Metals for Homogeneous Catalyzed Hydroformylation Reactions. *Angew. Chem., Int. Ed.* **2013**, *52*, 2852−2872. (b) Franke, R.; Selent, D.; Börner, A. Applied Hydroformylation. *Chem. Rev.* **2012**, *112*, 5675−5732. (c) Gil, W.; Trzeciak, A. M. N-Heterocyclic carbene−rhodium complexes as catalysts for hydroformylation and related reactions. *Coord. Chem. Rev.* **2011**, *255*, 473−483. (d) Hebrard, F.; Kalck, P. Cobalt-Catalyzed Hydroformylation of Alkenes: Generation and Recycling of the Carbonyl Species, and Catalytic Cycle. *Chem. Rev.* **2009**, *109*, 4272−4282. (e) Wiese, K.-D.; Obst, D. Hydroformylation. In *Catalytic Carbonylation Reactions*; Beller, M., Ed.; Springer: Berlin, Heidelberg, 2006; pp 1−33.

(2) Börner, A.; Franke, R. *Hydroformylation: Fundamentals, Processes, and Applications in Organic Synthesis*; Wiley-VCH: Weinheim, 2016.

(3) Orchin, M. $HCo(CO)_4$, the quintessential catalyst. *Acc. Chem. Res.* **1981**, *14*, 259−266.

(4) Slaugh, L. H.; Mullineaux, R. D. Novel Hydroformylation catalysts. *J. Organomet. Chem.* **1968**, *13*, 469−477.

(5) (a) Evans, D.; Osborn, J. A.; Wilkinson, G. Hydroformylation of alkenes by use of rhodium complex catalysts. *J. Chem. Soc. A* **1968**, 3133−3142. (b) Pruett, R. L.; Smith, J. A. Low-pressure system for producing normal aldehydes by hydroformylation of .alpha.-olefins. *J. Org. Chem.* **1969**, *34*, 327−330. (c) *Rhodium Catalyzed Hydroformylation*; van Leeuwen, P. W. N. M., Claver, C., Eds.; Kluwer Academic Publishers: Dordrecht, 2000.

(6) Ludwig, J. R.; Schindler, C. S. Catalyst: Sustainable Catalysis. *Chem.* **2017**, *2*, 313−316.

(7) Hood, D. M.; Johnson, R. A.; Carpenter, A. E.; Younker, J. M.; Vinyard, D. J.; Stanley, G. G. Highly active cationic cobalt(II) hydroformylation catalysts. *Science* **2020**, *367*, 542−548.

(8) Heck, R. F.; Breslow, D. S. The Reaction of Cobalt Hydrotetracarbonyl with Olefins. *J. Am. Chem. Soc.* **1961**, *83*, 4023−4027.

(9) Kégl, T. Computational aspects of hydroformylation. *RSC Adv.* **2015**, *5*, 4304−4327.

(10) Grima, J. P.; Choplin, F.; Kauffmann, G. Theoretical study of the hydroformylation reaction mechanism. *J. Organomet. Chem.* **1977**, *129*, 221−237.

(11) (a) Solà, M.; Ziegler, T. Theoretical Study on Acetaldehyde and Ethanol Elimination from the Hydrogenation of $CH_3(O)CCo-(CO)_3$. *Organometallics* **1996**, *15*, 2611−2618. (b) Versluis, L.; Ziegler, T.; Fan, L. A theoretical study on the insertion of ethylene into the cobalt−hydrogen bond. *Inorg. Chem.* **1990**, *29*, 4530−4536. (c) Versluis, L.; Ziegler, T.; Baerends, E. J.; Ravenek, W. Energetics of intermediates and reaction steps involved in the hydroformylation reaction catalyzed by HCo(CO)4. A theoretical study based on density functional theory. *J. Am. Chem. Soc.* **1989**, *111*, 2018−2025.

(12) Goh, S. K.; Marynick, D. S. The Carbonylation Reaction of $CH_3Co(CO)_4$: A Detailed Density Functional Study. *Organometallics* **2002**, *21*, 2262−2267.

(13) Huo, C.-F.; Li, Y.-W.; Beller, M.; Jiao, H. $HCo(CO)_3$-Catalyzed Propene Hydroformylation. Insight into Detailed Mechanism. *Organometallics* **2003**, *22*, 4665−4677.

(14) (a) Szlapa, E. N.; Harvey, J. N. Computational Modelling of Selectivity in Cobalt-Catalyzed Propene Hydroformylation. *Chem. - Eur. J.* **2018**, *24*, 17096−17104. (b) Rush, L. E.; Pringle, P. G.; Harvey, J. N. Computational Kinetics of Cobalt-Catalyzed Alkene Hydroformylation. *Angew. Chem., Int. Ed.* **2014**, *53*, 8672−8676.

(15) A focus of this DFT study is on establishing a general hydroformylation mechanism for the new class of cationic Co(II) catalysts, and the reaction of t-butylethylene is well-suited for the study because this alkene substrate has no isomerization side-reactions.

(16) Frisch, M. J.; Trucks, G. W.; Schlegel, H. B.; Scuseria, G. E.; Robb, M. A.; Cheeseman, J. R.; Scalmani, G.; Barone, V.; Men-nucci, B.; Petersson, G. A.; Nakatsuji, H.; Caricato, M.; Li, X.; Hratchian, H. P.; Izmaylov, A. F.; Bloino, J.; Zheng, G.; Sonnen-berg, J. L.; Hada, M.; Ehara, M.; Toyota, K.; Fukuda, R.; Hasegawa, J.; Ishida, M.; Nakajima, T.; Honda, Y.; Kitao, O.; Nakai, H.; Vreven, T.; Montgomery, J. A., Jr.; Peralta, J. E.; Ogliaro, F.; Bearpark, M.; Heyd, J. J.; Brothers, E.; Kudin, K. N.; Staroverov, V. N.; Kobayashi, R.; Normand, J.; Raghavachari, K.; Rendell, A.; Burant, J. C.; Iyengar, S. S.; Tomasi, J.; Cossi, M.; Rega, N.; Millam, J. M.; Klene, M.; Knox, J. E.; Cross, J. B.; Bakken, V.; Adamo, C.; Jaramillo, J.; Gomperts, R.; Stratmann, R. E.; Yazyev, O.; Austin, A. J.; Cammi, R.; Pomelli, C.; Ochterski, J. W.; Martin, R. L.; Morokuma, K.; Zakrzewski, V. G.; Voth, G. A.; Salvador, P.; Dannenberg, J. J.; Dapprich, S.; Daniels, A. D.; Farkas, O.; Foresman, J. B.; Ortiz, J. V.; Cioslowski, J.; Fox, D. J. *Gaussian 09*, rev. D.01; Gaussian Inc.: Wallingford, CT, 2013.

(17) Zhao, Y.; Truhlar, D. G. A new local density functional for main-group thermochemistry, transition metal bonding, thermochemical kinetics, and noncovalent interactions. *J. Chem. Phys.* 2006, *125*, 194101.

(18) (a) Andrae, D.; Häussermann, U.; Dolg, M.; Stoll, H.; Preuss, H. Energy-Adjusted ab initio Pseudopotentials for the Second and Third Row Transition Elements. *Theor. Chim. Acta* 1990, *77*, 123−141. (b) Dolg, M.; Wedig, U.; Stoll, H.; Preuss, H. Energy-Adjusted ab initio Pseudopotentials for the First Row Transition Elements. *J. Chem. Phys.* 1987, *86*, 866−872.

(19) Marenich, A. V.; Cramer, C. J.; Truhlar, D. G. Universal Solvation Model Based on Solute Electron Density and on a Continuum Model of the Solvent Defined by the Bulk Dielectric Constant and Atomic Surface Tensions. *J. Phys. Chem. B* 2009, *113*, 6378−6396.

(20) Dimethoxytetraglyme is not among the solvents that Gaussian 09 predefined for the SMD model, so the closest predefined solvent THF was used instead.

(21) (a) Benson, S. W. *The Foundations of Chemical Kinetics*; R. E. Krieger: Malabar, FL, 1982. (b) Schoenebeck, F.; Houk, K. N. Ligand-Controlled Regioselectivity in Palladium-Catalyzed Cross Coupling Reactions. *J. Am. Chem. Soc.* 2010, *132*, 2496−2497. (c) Liu, B.; Gao, M.; Dang, L.; Zhao, H.; Marder, T. B.; Lin, Z. DFT Studies on the Mechanisms of the Platinum-Catalyzed Diboration of Acyclic $\alpha$, $\beta$-Unsaturated Carbonyl Compounds. *Organometallics* 2012, *31*, 3410−3425. (d) Zhou, Q.; Li, Y. The Real Role of N-Heterocyclic Carbene in Reductive Functionalization of $CO_2$: An Alternative Understanding from Density Functional Theory Study. *J. Am. Chem. Soc.* 2015, *137*, 10182−10189.

(22) [Co(PP)(acac)]$^+$ (**CAT1**) has been calculated as a low-spin (doublet) and high-spin (quartet) complex, respectively; the low-spin complex is lower in energy by 3.0 kcal/mol.

(23) The doublet and the quartet of the active species [HCo(CO)$_2$(PP)]$^+$ (**IM3/IM4/IM6**) have been calculated with M06-L and M06. Both methods predict the doublet to be much more stable (Figure S1).

(24) Grimme, S.; Antony, J.; Ehrlich, S.; Krieg, H. Krieg, H. A consistent and accurate ab initio parametrization of density functional dispersion correction (DFT-D) for the 94 elements H−Pu. *J. Chem. Phys.* 2010, *132*, 154104−154119.

(25) Zhao, Y.; Truhlar, D. G. The M06 suite of density functionals for main group thermochemistry, thermochemical kinetics, non-covalent interactions, excited states, and transition elements: two new functionals and systematic testing of four M06-class functionals and 12 other functionals. *Theor. Chem. Acc.* 2008, *120*, 215−241.

(26) Bungu, P. N.; Otto, S. Bicyclic phosphines as ligands for cobalt catalysed hydroformylation. Crystal structures of [Co(Phoban[3.3.1]-Q)(CO)$_3$]$_2$ (Q = C$_2$H$_5$, C$_5$H$_{11}$, C$_3$H$_6$NMe$_2$, C$_6$H$_{11}$). *Dalton Trans.* 2007, 2876−2884.

(27) The alkene $\pi$-complexes could not be located.

(28) (a) Kozuch, S.; Shaik, S. A combined kinetic−quantum mechanical model for assessment of catalytic cycles: Application to cross-coupling and Heck reactions. *J. Am. Chem. Soc.* 2006, *128*, 3355−3365. (b) Kozuch, S.; Shaik, S. How to Conceptualize Catalytic Cycles? The Energetic Span Model. *Acc. Chem. Res.* 2011, *44*, 101−110.

(29) Li, P.; Shen, C.; Min, J.; Mei, J.-Y.; Zheng, H.; He, L.; Tian, X. Computational investigation of the ligand effect on the chemo/regioselectivity and reactivity of cobalt-catalysed hydroformylation. *Catal. Sci. Technol.* 2020, *10*, 2994−3007.

(30) For normal alkenes like 1-hexene, the catalyst was found to be less regioselective by the experimentalists. See ref 7 and results therein.

(31) Whyman, R. The hydroformylation of olefins catalysed by cobalt carbonyls: a high pressure infrared spectral study. *J. Organomet. Chem.* 1974, *81*, 97−106.

(32) A 1:1 **CAT1**:PMe$_3$ mole ratio has been assumed for the calculations. Use of a catalytic amount of PMe$_3$ is suggested for experimental tests.